Analysis of Hybrid Cable-Thruster actuated ROV in heavy lifting interventions

Nikolas Sacchi, Enrico Simetti, Gianluca Antonelli, Giovanni Indiveri, Vincent Creuze, Marc Gouttefarde

Analysis of Hybrid Cable-Thruster actuated ROV in heavy lifting interventions*

Nikolas Sacchi, Enrico Simetti, Gianluca Antonelli, Giovanni Indiveri, Vincent Creuze, Marc Gouttefarde

***Abstract*— Many operations performed by work class Remotely Operated Vehicles (ROVs) require the manipulation of heavy loads. An example is the manipulation and grouting of armour stones. A way to increase the working capabilities of the ROV is to introduce cables among the set of actuators. The cable lengths and tensions are controlled by winches placed on the vehicle. Being similar to a cable-driven parallel robot (CDPR), the resultant system inherits some advantages such as the possibility to generate large forces over a large workspace and the possibility to use CDPR techniques to estimate the pose of the ROV. This paper proposes a complete control architecture for the Hybrid Cable-Thruster actuated ROV (HCT-ROV) and analyzes, in computer simulations, the performances of such a system while it performs real world operations, such as heavy lifting and hovering in presence of water current.**

I. INTRODUCTION

Remotely Operated Vehicles (ROVs) are employed in several fields such as offshore oil and gas industry, defence, maritime search and rescue, scientific research, deep sea mining and many others [1]. An ROV is an underwater vehicle physically linked to an operator who is, for example, on a surface vessel. The connection is done via an umbilical cable, which transfers power to the vehicle and closes the manned loop [2]. Many of the operations that ROVs usually perform require the grasping and the manipulation of heavy payloads. An example of such operations is the manipulation and grouting of pre-placed armour stones, which are used nearshore and offshore to protect seabed from erosion. Due to the weight of the armor stones, ROVs with high working capabilities must be employed. In general, underwater vehicles are actuated by thrusters, which define the working capabilities of the vehicle. The maximum payload of an ROV can be increased either by installing more thrusters or by using more powerful ones. Unfortunately, these choices would result in a significantly increased cost and design complexity. A solution to this problem has been proposed in [3]. The authors presented an underwater robotic platform composed by an Underwater Vehicle-Manipulator System (UVMS) actuated in a hybrid fashion by thrusters and cables. The choice of actuating the vehicle using cables is inspired by Cable-Driven Parallel Robots (CDPR) [4], which consist of a fixed base and a moving platform driven by cables whose lengths and tensions are controlled by a set of winches. Due to their structure, cables allows the transmission of motion and force from the fixed platform to the moving one over large distances. Therefore, CDPRs are notably characterized by large workspaces, e.g. [5], [6]. This characteristic makes the introduction of cables among the actuators of an underwater vehicle a good solution for increasing its working capabilities, still maintaining a large workspace. Besides, the presence of cables, which can be considered as straight-line segments when large enough cable tensions is maintained with the winches, allows to use CDPR methodologies such as [7], [8] to estimate the position and attitude of the ROV in a more precise way compared to systems such as a long baseline acoustic localization [9] associated with an inertial navigation system. However, in [3] only a proof of concept of the system has been provided, analyzing the performance of the system in simple, planar scenarios (3 DOFs).

Expanding the work done in [3], the present paper analyzes the performance of an Hybrid Cable-Thruster actuated ROV (HCT-ROV) performing heavy lifting operations. Differently from [3], the cables are not considered as ideal force generators but they are treated as multibody dynamic systems which are able to generate a force only in certain conditions. In particular, a cable is considered as an actuator only if it is straight, i.e., the bodies that compose it are aligned. Besides, the robotic system moves in a spatial environment (6 DOFs) interacting with external objects. Moreover, we propose a complete control architecture for the HCT-ROV. Starting from a reference configuration for the underwater vehicle, reference forces/moments are generated. Then, according to maximum actuation capabilities, forces among the different actuators are allocated using a control allocation methodology based on Quadratic Programming (QP). Since a prototype of the HCT-ROV has not been built yet (and, to the best of our knowledge, there is no HCT-ROV prototype in the state of the art), the system has been virtualized in Vortex Studio, a multibody real-time simulation software. The choice of this simulator is motivated by its capability of simulating interactions between rigid bodies and fluids and by the accuracy in the simulation of flexible cable dynamics. Specifically, the HCT-ROV is tested in two simulated real case scenarios, namely heavy payload lifting and hovering in presence of water current.

The paper is organized as follows. Section II provides a description of the kinematics and the dynamics of the

*This work has received funding from the University of Genova through the BIPE 2020 call (CableROV project) with the support of the Fondazione Compagnia San Paolo

N. Sacchi is with DIII, Univ Pavia, Pavia, Italy {nikolas.sacchi01@universitadipavia.it}

E. Simetti and G. Indiveri are with DIBRIS, Univ Genova, Genova, Italy {enrico.simetti@unige.it, giovanni.indiveri@unige.it}

G. Antonelli is with DIEI, Univ Cassino, Cassino, Italy {antonelli@unicas.it}

V. Creuze, and M. Gouttefarde, are with LIRMM, Univ Montpellier, CNRS, Montpellier, France {vincent.creuze@lirmm.fr, marc.gouttefarde@lirmm.fr }

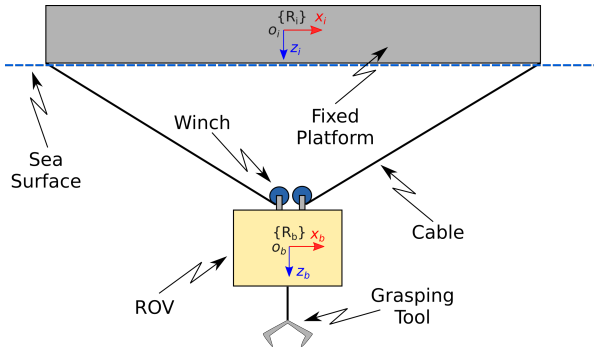

Fig. 1: A 2D representation of the system. The ROV is suspended by cables under a fixed structure.

system. In Section III, the components of the complete control architecture are described. In Section IV, the dynamic parameters of the virtualized system, along with a description of the system actuators and effectors, are given. Section V describes the simulations made to test the HCT-ROV and analyzes the results. Finally, in Section VI conclusions are made and future work is presented.

II. SYSTEM DESCRIPTION AND MODELING

The HCT-ROV is a robotic system composed by an ROV connected by means of n_C flexible cables to a platform placed out of the water. In this work, the position of the platform is assumed not to be affected by the oscillatory motion of the waves, i.e., it is fixed. This assumption is reasonable when the HCT-ROV operates in a good weather conditions and calm sea. The cable lengths and tensions are controlled by a set of n_C winches mounted on the vehicle. In order to minimize the number of cables deployed in the water, we choose to have $n_C < 6$. This fact makes fundamental the presence of thrusters since, with cable actuation only, the underwater vehicle would be under actuated so that the full control of its motions would not be possible or significantly more complex. Besides, note that if the vehicle is fully actuated by thrusters, the introduction of cables leads to actuation redundancy, making the system *overactuated*.

In the system, two different reference frames can be identified: An inertial frame $\{\mathcal{R}_i\}$ attached to the center of volume of the fixed platform and a body-fixed frame $\{\mathcal{R}_b\}$, attached to the vehicle center of mass. The former one is oriented with the z_i axis point downward, the latter is oriented with the x_b axis pointing forward and the z_b axis pointing downward, as depicted in Fig. 1.

A. Kinematics

The pose $\boldsymbol{\eta} \in \mathbb{R}^6$ of the vehicle is the combination of its position and orientation (expressed in terms of *roll* ϕ, *pitch* θ and *yaw* ψ angles) with respect to $\{\mathcal{R}_i\}$. In particular, according to the SNAME notation detailed in [10], $\boldsymbol{\eta} = \begin{bmatrix} x_i & y_i & z_i & \phi & \theta & \psi \end{bmatrix}^\top$.

Since cables are introduced and, as explained at the end of Section II-B, they are kept straight by a torque applied to the winches, it is possible to treat the system as a CDPR and thus to estimate the pose of the vehicle from the cable lengths by solving the forward kinematics problem. Differently from serial robots, solving the forward kinematics of a parallel robot is not trivial and different techniques can be used, e.g., the one introduced in [11]. In particular, given a set of cable lengths l_k, with $k = 1, ..., n_C$, this technique uses Levemberg-Marquardt (LM) [12] optimization to solve the nonlinear problem

$$\min_{x_i, y_i, z_i, \phi, \theta, \psi} \sum_{k=1}^{n_C} \Psi_k(l_k, x_i, y_i, z_i, \phi, \theta, \psi). \tag{1}$$

where

$$\Psi_k = (||\boldsymbol{r}_{pl_k} - \boldsymbol{\eta}_1 - \boldsymbol{R}_b^i(\phi, \theta, \psi)\boldsymbol{s}_{rov_k}||_2)^2 - l_k^2 \tag{2}$$

with $\boldsymbol{\eta}_1 = \begin{bmatrix} x_i & y_i & z_i \end{bmatrix}^\top$ being the position of the ROV in the inertial frame $\{\mathcal{R}_i\}$, $\boldsymbol{r}_{pl_k} \in \mathbb{R}^3$ the position (expressed in frame $\{\mathcal{R}_i\}$) of the kth cable endpoint on the fixed platform, $\boldsymbol{s}_{rov_k} \in \mathbb{R}^3$ the position of the kth cable endpoint on the vehicle expressed in frame $\{\mathcal{R}_b\}$ and $\boldsymbol{R}_b^i(\phi, \theta, \psi) \in \mathbb{R}^{3\times3}$ the rotation matrix that expresses the orientation of frame $\{\mathcal{R}_b\}$ with respect to frame $\{\mathcal{R}_i\}$.

B. Underwater Vehicle Dynamics

The dynamic simulator used to virtualized the proposed HCT-ROV system, i.e., Vortex Studio, implements the dynamics of underwater vehicles. For completeness, based on [13], a brief description of underwater vehicle dynamics is presented in the following.

Assuming that the vehicle is moving with a velocity $\boldsymbol{\nu} = \begin{bmatrix} u & v & w & p & q & r \end{bmatrix}^\top$ (expressed in frame $\{\mathcal{R}_b\}$) while being subject to a constant and irrotational current which has velocity $\boldsymbol{v}_C^i = \begin{bmatrix} v_x & v_y & v_z \end{bmatrix}^\top$ (expressed in frame $\{\mathcal{R}_i\}$), the dynamics of the ROV can be expressed by

$$\dot{\boldsymbol{\eta}} = \boldsymbol{J}(\boldsymbol{\eta})\,\boldsymbol{\nu}_r + \begin{bmatrix} \boldsymbol{v}_C^i \\ \boldsymbol{0}_{3\times1} \end{bmatrix} \tag{3a}$$

$$\boldsymbol{M}\dot{\boldsymbol{\nu}}_r + \boldsymbol{C}(\boldsymbol{\nu}_r)\boldsymbol{\nu}_r + \boldsymbol{D}(\boldsymbol{\nu}_r)\boldsymbol{\nu}_r + \boldsymbol{g}(\boldsymbol{\eta}) = \boldsymbol{\tau}_a + \boldsymbol{\tau}_{ext} \tag{3b}$$

where $\boldsymbol{\nu}_r = \boldsymbol{\nu} - \begin{bmatrix} \boldsymbol{R}_i^b \boldsymbol{v}_C^i & \boldsymbol{0}_{1\times3} \end{bmatrix}^\top$ is the relative velocity between the vehicle and the fluid, $\boldsymbol{J}(\boldsymbol{\eta}) \in \mathbb{R}^{6\times6}$ is the vehicle Jacobian, $\boldsymbol{M} = \boldsymbol{M}_{RB} + \boldsymbol{M}_A \in \mathbb{R}^{6\times6}$ takes into account the rigid body inertia and the added mass, $\boldsymbol{C}(\boldsymbol{\nu}_r) = \boldsymbol{C}_{RB}(\boldsymbol{\nu}_r) + \boldsymbol{C}_A(\boldsymbol{\nu}_r) \in \mathbb{R}^{6\times6}$ represents the Coriolis and centripetal effects, including added masses effects, $\boldsymbol{D}(\boldsymbol{\nu}_r) \in \mathbb{R}^{6\times6}$ is the matrix of the damping coefficients, $\boldsymbol{g}(\boldsymbol{\eta}) \in \mathbb{R}^6$ is the vector of the restoring force due to gravity and buoyancy, $\boldsymbol{\tau}_{ext} \in \mathbb{R}^6$ is the set of forces/moments generated by external disturbances, which also includes the unmodeled inertial effects of the current on the added masses.

The HCT-ROV is actuated by n_T thrusters and n_C cables, which generate forces on the underwater vehicle. These forces are gathered in vectors $\boldsymbol{f}_T \in \mathcal{F}_T$ and $\boldsymbol{f}_C \in \mathcal{F}_C$, respectively, where the sets $\mathcal{F}_T$ and $\mathcal{F}_C$ are defined as

$$\mathcal{F}_T = \{\boldsymbol{f}_T \in \mathbb{R}^{n_T} \mid \underline{\boldsymbol{f}}_T \preccurlyeq \boldsymbol{f}_T \preccurlyeq \overline{\boldsymbol{f}}_T\} \tag{4a}$$

$$\mathcal{F}_C = \{\boldsymbol{f}_C \in \mathbb{R}^{n_C} \mid \underline{\boldsymbol{f}}_C \preccurlyeq \boldsymbol{f}_C \preccurlyeq \overline{\boldsymbol{f}}_C\}. \tag{4b}$$

The operator $\preccurlyeq$ represents the component-wise inequality operation, while $\underline{\boldsymbol{f}}_T$, $\underline{\boldsymbol{f}}_C$, $\overline{\boldsymbol{f}}_T$ and $\overline{\boldsymbol{f}}_C$ are the lower and upper bounds for the thrusters and cable forces.

The set of forces and moments that is exerted on the ROV due to the action of thrusters and cables depends on the *thruster configuration matrix* $\boldsymbol{B}_T \in \mathbb{R}^{6\times n_T}$ and on the *cable wrench matrix* $\boldsymbol{B}_C \in \mathbb{R}^{6\times n_C}$, defined as

$$\boldsymbol{B}_T = \begin{bmatrix} \hat{\boldsymbol{u}}_{t_1} & \dots & \hat{\boldsymbol{u}}_{t_{n_T}} \\ \boldsymbol{s}_{t_1} \times \hat{\boldsymbol{u}}_{t_1} & \dots & \boldsymbol{s}_{t_{n_T}} \times \hat{\boldsymbol{u}}_{t_{n_T}} \end{bmatrix} \tag{5a}$$

$$\boldsymbol{B}_C = \begin{bmatrix} \hat{\boldsymbol{u}}_{c_1} & \dots & \hat{\boldsymbol{u}}_{c_{n_C}} \\ \boldsymbol{s}_{c_1} \times \hat{\boldsymbol{u}}_{c_1} & \dots & \boldsymbol{s}_{c_{n_C}} \times \hat{\boldsymbol{u}}_{c_{n_C}} \end{bmatrix} \tag{5b}$$

where the unit vectors $\hat{\boldsymbol{u}}_{t_i} \in \mathbb{R}^3$ and $\hat{\boldsymbol{u}}_{c_k} \in \mathbb{R}^3$ represent the direction of the forces generated by the ith thruster and the kth cable, $\boldsymbol{s}_{t_i} \in \mathbb{R}^3$ is the position of the ith thruster and $\boldsymbol{s}_{c_k} \in \mathbb{R}^3$ is the position of the kth cable endpoint on the ROV. All these quantities are expressed with respect to frame $\{\mathcal{R}_b\}$.

Defining the *actuator wrench matrix* $\boldsymbol{B} = \begin{bmatrix} \boldsymbol{B}_T & \boldsymbol{B}_C \end{bmatrix}$ and the set of the actuator forces $\boldsymbol{f}_a = \begin{bmatrix} \boldsymbol{f}_T^\top & \boldsymbol{f}_C^\top \end{bmatrix}^\top$, allows to express the set of forces and moments (wrenches) that the actuators exert on the ROV as

$$\boldsymbol{\tau}_a = \boldsymbol{B}\, \boldsymbol{f}_a. \tag{6}$$

It is important to note that, due to their mechanical structure, cables can generate unilateral forces only, pulling the ROV toward the fixed platform, therefore $\underline{\boldsymbol{f}}_C = 0$. However, in order to maintain the cable straight, a strictly positive lower bound, whose value is related to the ROV dimensions and weight, is set ($\underline{\boldsymbol{f}}_C > 0$).

C. Flexible Cable Modeling

All the cables of the proposed HCT-ROV have been treated as multibody systems discretized using *lumped element model*, as detailed in [14]. Each cable is considered as a system of several rigid-body links interconnected by cylindrical joints. Each joint is modeled as a set of three linear constraint equations and a set of three angular constraint equations, which constrain the relative linear and angular motion of the elements of the cable. Depending on the parameters of the constraint equations, different elastic properties can be simulated.

III. CONTROL ARCHITECTURE

A. Reference Generation

Given a reference configuration $\boldsymbol{\eta}^* \in \mathbb{R}^6$ for the ROV and its current configuration $\boldsymbol{\eta} \in \mathbb{R}^6$ at time instant t, a reference velocity $\boldsymbol{\nu}^* = \begin{bmatrix} (\boldsymbol{\nu}_1^*)^\top & (\boldsymbol{\nu}_2^*)^\top \end{bmatrix}^\top \in \mathbb{R}^6$, expressed in frame $\{\mathcal{R}_b\}$, can be computed as follows. The reference linear linear velocity $\boldsymbol{\nu}_1^* \in \mathbb{R}^3$ can be computed as

$$\boldsymbol{\nu}_1^* = \boldsymbol{R}_i^b(\phi, \theta, \psi)\, [\boldsymbol{K}_{P_\nu}(\boldsymbol{\eta}_1^* - \boldsymbol{\eta}_1)] \tag{7}$$

where $\boldsymbol{K}_{P_\nu} \in \mathbb{R}^{3\times 3}$ is a diagonal matrix of gains, $\boldsymbol{R}_i^b \in \mathbb{R}^{3\times 3}$ is the rotation matrix describing the orientation of frame $\{\mathcal{R}_i\}$ with respect to frame $\{\mathcal{R}_b\}$, while $\boldsymbol{\eta}_1 \in \mathbb{R}^3$ is the position of the ROV with respect to frame $\{\mathcal{R}_i\}$. The reference angular velocity $\boldsymbol{\nu}_2^* \in \mathbb{R}^3$ is computed in three steps. First, the rotation matrix which expresses the orientation of the desired configuration with respect to the body-fixed frame $\{\mathcal{R}_b\}$ is defined as

$$\boldsymbol{R}_{ref}^b = \boldsymbol{R}_i^b(\phi, \theta, \psi) \boldsymbol{R}_{ref}^i(\phi^*, \theta^*, \psi^*). \tag{8}$$

Then, the *matrix logarithm* operation is carried out to obtain the angle axis representation of the angular velocity which would bring the frame $\{\mathcal{R}_b\}$ to the desired orientation in one second [15]. In particular, the axis of rotation is specified by the unit vector $\hat{\boldsymbol{\omega}} \in \mathbb{R}^3$, while the angular velocity is expressed in rad/s and denoted as $\alpha \in \mathbb{R}$. Finally, the reference angular velocity is computed as $\boldsymbol{\nu}_2^* = k_\nu\, \alpha\, \hat{\boldsymbol{\omega}}$, where $k_\nu \in \mathbb{R}$ is a constant gain.

The reference velocity $\boldsymbol{\nu}^*$ is then used to generate a reference signal for the set of forces and moments $\boldsymbol{\tau}_a^* \in \mathbb{R}^6$ using

$$\boldsymbol{\tau}_a^* = \boldsymbol{K}_{P_\tau}(\boldsymbol{\nu}^* - \boldsymbol{\nu}) + \boldsymbol{K}_{I_\tau} \int_0^t (\boldsymbol{\nu}^* - \boldsymbol{\nu})\, dt \tag{9}$$

where $\boldsymbol{\nu} \in \mathbb{R}^6$ is the ROV velocity expressed in frame $\{\mathcal{R}_b\}$ at time instant t, while $\boldsymbol{K}_{P_\tau} \in \mathbb{R}^{6\times 6}$ and $\boldsymbol{K}_{I_\tau} \in \mathbb{R}^{6\times 6}$ are diagonal matrices of proportional and integral gains.

The contribution of the load attached to the ROV must also be considered in the generation of the reference $\boldsymbol{\tau}_a^*$. Assuming that the load is attached using a hook and a cable, it is then possible to measure the cable tension $t_l \in \mathbb{R}$ and approximate the force (expressed in frame $\{\mathcal{R}_b\}$) exerted on the vehicle by the load as a linear force given by $\boldsymbol{f}_l \approx \boldsymbol{R}_i^b \begin{bmatrix} 0 & 0 & t_l \end{bmatrix}^\top \in \mathbb{R}^3$. Moreover, assuming that the cable with the hook is attached to the ROV in $\boldsymbol{s}_l \in \mathbb{R}^3$ (expressed in $\{\mathcal{R}_b\}$), then the total contribution of the load that must be added to the reference set of forces and moments (9) can be approximated $\boldsymbol{\tau}_{load} \approx \begin{bmatrix} \boldsymbol{f}_l^\top & (\boldsymbol{s}_l \times \boldsymbol{f}_l)^\top \end{bmatrix}^\top \in \mathbb{R}^6$.

B. Control Allocation

The unidirectional nature of the cable forces and the fact that the system is overactuated ($n_C + n_T > 6$) impose the use of particular control allocation methodologies to generate the set of actuator forces $\boldsymbol{f}_a^* \in \mathbb{R}^{n_{act}}$ given a set of desired forces and moments $\boldsymbol{\tau}_a^* \in \mathbb{R}^6$. In the literature, several methodologies have been presented in [16], [17], [18], [19].

Due to the nature of the system under consideration and the presence of actuator constraints (4), it is convenient to formulate the HCT-ROV control allocation problem as a QP problem [20] as it follows

$$\min_{\boldsymbol{f}_a^*} \quad \frac{1}{2}(\boldsymbol{f}_a^*)^\top\, \boldsymbol{Q}\, \boldsymbol{f}_a^* \tag{10a}$$

$$\text{subject to} \quad \boldsymbol{B}\, \boldsymbol{f}_a^* = \boldsymbol{\tau}_a^*, \tag{10b}$$

$$\boldsymbol{f}_a^* \preccurlyeq \overline{\boldsymbol{f}}_a \tag{10c}$$

$$-\boldsymbol{f}_a^* \preccurlyeq -\underline{\boldsymbol{f}}_a \tag{10d}$$

where $\boldsymbol{f}_a^* = \begin{bmatrix} (\boldsymbol{f}_T^*)^\top & (\boldsymbol{f}_C^*)^\top \end{bmatrix}^\top \in \mathbb{R}^{n_{act}}$ is the optimization variable vector, $\boldsymbol{Q} = \boldsymbol{Q}^T \in \mathbb{R}^{n_{act}\times n_{act}}$ is the Hessian matrix of the objective function, $\boldsymbol{B}$ is the actuator wrench matrix, while $\underline{\boldsymbol{f}}_a = \begin{bmatrix} \underline{\boldsymbol{f}}_T^\top & \underline{\boldsymbol{f}}_C^\top \end{bmatrix}^\top$ and $\overline{\boldsymbol{f}}_a =$

$\begin{bmatrix}\underline{\boldsymbol{f}}_T^\top & \underline{\boldsymbol{f}}_C^\top\end{bmatrix}^\top$ are the lower and upper bounds on the HCT-ROV actuator forces. From a practical point of view, the matrix $\boldsymbol{Q}$ weights the usage of each actuator, i.e., $\boldsymbol{Q} = \text{diag}\{q_1, \dots, q_{n_T}, q_{n_T+1}, \dots q_{n_T+n_C}\}$, where each weight q_i can be defined based on some user-defined preferences. Once the QP problem is formulated, it can be solved using well-known approaches like the ones proposed in [21], [22].

In some situations, a feasible solution for the QP problem (10) may not exist. From a practical perspective, it means that the desired set of forces and moments $\boldsymbol{\tau}_a^*$ cannot be generated because it is greater than the maximum set of forces and moments that can be generated by the actuators. A solution, used in the simulations presented in Section V, consists in finding the largest set of forces and moments $\overline{\gamma}\,\boldsymbol{\tau}_a^*$, with $\overline{\gamma} \in (0, 1]$, which can be generated by the actuators. The QP problem (10) is then reformulated by substituting (10b) with

$$\boldsymbol{B}\,\boldsymbol{f}_a^* = \overline{\gamma}\,\boldsymbol{\tau}_a^*. \tag{11}$$

The value of $\overline{\gamma}$ can be found in several ways. A very simple approach is to solve the modified version of the QP, changing $\overline{\gamma}$ according to the bisection method when a feasible solution does not exist.

IV. CASE STUDY

The aim of this section is to describe the process of virtualization of the HCT-ROV inside the simulation environment, i.e., Vortex Studio, which implements the underwater vehicle dynamics and the cable dynamics presented in Section II-C.

A. Vortex Heavy Work Class ROV

The underwater vehicle considered in the system, depicted in Fig. 2, is the *Vortex Heavy Work Class ROV*: A heavy ROV designed and virtualized by CM Labs in Vortex Studio. The ROV has dimensions equal to 2.28 m $\times$ 1.7 m $\times$ 1.9 m along its x, y and z axes. All the dynamical parameters of the vehicle are provided by the simulator. The mass of the ROV is 3975 kg, the moments of inertia about its principal axes are $I_{xx} = 2120.38$ kg $\cdot$ m^2, $I_{yy} = 3453.13$ kg $\cdot$ m^2 and $I_{zz} = 3155.3$ kg $\cdot$ m^2, the position of the center of mass and of the center of buoyancy, with respect to the frame $\{\mathcal{R}_b\}$, are $\boldsymbol{s}_{cm} = \begin{bmatrix}0 & 0.05 & 0.026\end{bmatrix}^\top$ (m) and $\boldsymbol{s}_{cb} = \begin{bmatrix}0 & 0.05 & -0.333\end{bmatrix}^\top$ (m), the added mass matrix is $\boldsymbol{M}_A = -diag\{-380 \text{ kg}, -380 \text{ kg}, -380 \text{ kg}, -600 \text{ kg} \cdot \text{m}^2, -600 \text{ kg} \cdot \text{m}^2, -600 \text{ kg} \cdot \text{m}^2\}$ while the (dimensionless) drag coefficient along x_b, y_b and z_b are 3.25, 3.8 and 3.2.

B. System Actuators

The virtualized HCT-ROV is actuated by $n_T = 7$ thrusters and $n_C = 4$ cables. In the simulator, each thruster is modeled as an ideal force generator, thus if at time t a force f_{t_i} is requested to the ith thruster, at time $t + dt$ this force will be provided. The bounds on the forces generated by the thrusters are $\underline{\boldsymbol{f}}_T = \begin{bmatrix}-3372 & -3372 & \dots & -3372\end{bmatrix}^\top$ (N) and $\overline{\boldsymbol{f}}_T = \begin{bmatrix}3800 & 3800 & \dots & 3800\end{bmatrix}^\top$ (N).

The cables in the system, arranged as in Fig 1, are modeled as presented in Section II-C. Specifically, they

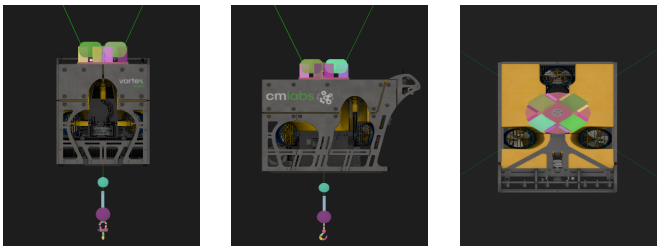

(a) Front view (b) Side view (c) Top view

Fig. 2: Views of the Vortex Heavy Work Class ROV in Vortex Studio together with its hooking system.

are composed by elements with length equal to 0.2 m and characterized by a Young's modulus equal to $3.5\text{N}/\text{m}^2$, a diameter of 0.02 m, and, to make them neutrally buoyant, a volumetric density equal to 1000 kg$/$m^3. The lengths of the cables and the forces that they exert on the ROV are controlled by a set of winches with drum radius $r = 0.15$ m mounted on the underwater vehicle. Specifically, if a force f_{c_k} needs to be generated by the kth cable and the cable is straight, then that force can be obtained by controlling the corresponding winch with a torque equal to $t_k = f_{c_k}\, r$. The maximum torque that each winch can deliver is 1500 Nm, therefore $\overline{\boldsymbol{f}}_C = \begin{bmatrix}10^4 & 10^4 & \dots & 10^4\end{bmatrix}^\top$. Furthermore, in order to maintain the cables straight at each time step, $\underline{\boldsymbol{f}}_C = \begin{bmatrix}150 & 150 & \dots & 150\end{bmatrix}^\top$ (N) has been found to be suitable.

C. System effectors

In the virtualized system, the dynamics of the grasping operation, along with all the complications that it implies, are not considered. In particular, the HCT-ROV is provided with a hooking system, as shown in Fig. 2. A load is considered grasped when the distance between the hook and a predefined hooking point on the load is smaller than 0.1 m. At each time step, the force that the load exerts on the vehicle can be estimated by measuring the tension of the cable which connects the hook to the ROV.

V. SIMULATIONS AND RESULTS

A. Simulations

To test the proposed HCT-ROV system, two different sets of simulations are considered. In the first set, the HCT-ROV executes a heavy load pick and place operation: it must reach a load, pick it using the hooking system, pass through a sequence of points, place it and then move to a predefined position. The points that the vehicle must reach, along with the type of action that it must perform at each of them, are given in Table I. The simulation has been repeated for different values of the load mass, specifically $m_l = \{700, 800, 900, 1000, 1500, 2000\}$ (kg) and, for each value of m_l, the HCT-ROV is controlled one time using only thrusters and one time using thrusters and cables. The aim of the second set of simulations is to test the hovering capabilities of the HCT-ROV in presence of water current. Specifically, the vehicle must remain at a predefined

TABLE I: Reference points and actions for the pick and place operation. All the points are expressed in frame $\{\mathcal{R}_i\}$.

INDEX	x_i [m]	y_i [m]	z_i [m]	ACTION
1	-4	4	22	PASS THROUGH
2	-4	4	24.5	PICK LOAD
3	-4	4	22	PASS THROUGH
4	3	3	22	PASS THROUGH
5	3	0	22	PASS THROUGH
6	-3	0	22	PASS THROUGH
7	-3	-3	22	PASS THROUGH
8	4	-4	22	PASS THROUGH
9	4	-4	24.5	PLACE LOAD
10	0	0	22	REACH AND STOP

position $\boldsymbol{r}_{ref} = \begin{bmatrix} 0 & 0 & 5 \end{bmatrix}^\top$ (m) while it is subject to a water current of velocity $\boldsymbol{v}_C^i = \begin{bmatrix} k_c & -k_c & 0 \end{bmatrix}^\top$ (m/s). Both the desired position and the current velocity are expressed in frame $\{\mathcal{R}_i\}$. The simulation has been repeated for $k_c = \{0.55, 0.65, 0.75\}$ (m/s), and, for each value of k_c the HCT-ROV is controlled one time using thrusters only and one time using both thrusters and cables. In order to perform fair comparisons, in all the simulations, the true pose of the vehicle is retrieved directly from the simulator. In the simulations in which the ROV is controlled by both cables and thrusters the control allocation has been performed solving the QP problem (10) with the equality constraint (11), selecting $\overline{\gamma}$ according to the bisection method, while the weights of the matrix $\boldsymbol{Q}$ are selected to always prioritize the usage of cables, i.e., $q_i = 1 \ \forall i = 1, 2, \ldots, n_T$ and $q_i = 0.1 \ \forall i = n_T + 1, n_T + 2, \ldots, n_T + n_C$. If the ROV is controlled using thrusters only, the same QP problem is solved, but $\boldsymbol{f}_a^* \in \mathbb{R}^{n_T}$, $\underline{\boldsymbol{f}}_a = \underline{\boldsymbol{f}}_T$, $\overline{\boldsymbol{f}}_a = \overline{\boldsymbol{f}}_T$, $\boldsymbol{Q} = \boldsymbol{I}_{n_T \times n_T}$ and $\boldsymbol{B} = \boldsymbol{B}_T$. The QP problem is solved using the C++ library ALGLIB [23]. Each simulation has a time step $dt = 0.0167$ s while the controller gains have been chosen as $\boldsymbol{K}_{P_\nu} = \text{diag}\{1.5, 1.5, 1.5\}$, $\boldsymbol{K}_{P_\tau} = \text{diag}\{2 \cdot 10^4, \ldots, 2 \cdot 10^4\}$, $\boldsymbol{K}_{I_\tau} = \text{diag}\{2 \cdot 10^3, \ldots, 2 \cdot 10^3\}$, $k_\nu = 1$. At each time step, the velocity of the ROV, its depth, its attitude and the cable lengths are available to the controller.

B. Results

The effectiveness of the HCT-ROV during heavy lifting operations has been assessed by evaluating the percentage of completion of the task, i.e., the number of points of Table I that have been reached. As shown in Fig. 3, when the underwater vehicle is actuated by thrusters only, it completes the task in 60 s and 66 s when $m_l \leq 800$ kg, but it fails otherwise. Failure, defined as the inability to pass through all the points in a finite time, happens because, when the load is too heavy, the thrusters are not able to generate the wrench necessary to transport it, hindering the ROV movements after the picking action. The situation changes when the underwater vehicle is actuated using both thrusters and cables. In fact, the HCT-ROV is able to complete the task in less than 58 s for all the load mass values that have been tested, showing that the introduction of cables significantly increases the lifting capabilities of the ROV.

The capability of the system to perform hovering operation

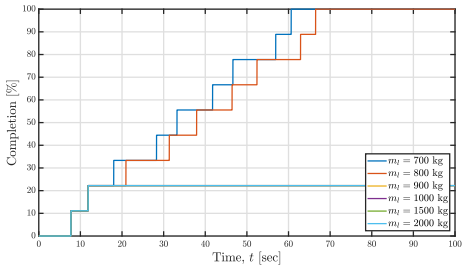

Fig. 3: Completion of the pick and place operation when the underwater vehicle is actuated only by thrusters.

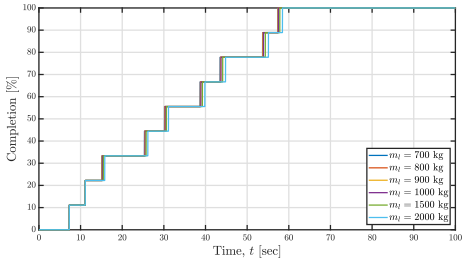

Fig. 4: Completion percentage of the pick and place operations (actuation by thrusters and cables).

in presence of water current has been evaluated by studying the time evolution of the underwater vehicle position. As illustrated in Fig. 5 and 6, when the underwater vehicle is actuated with thrusters and cables, it is less influenced by the presence of current. In particular, when it is controlled using thrusters only, the hovering operation is performed successfully only when $k_c = 0.55$, with steady state errors equal to 0.138 m, -0.138 m and 0.001 m along axes x_i, y_i and z_i, respectively. In the other cases, the thrusters on the ROV are not able to counteract the effect of the ocean current, making the vehicle drifting away from the hovering position. On the other hand, when the ROV is controlled by both cables and thrusters, it stays at the desired hovering position for all the tested values of k_c, with steady state errors indicated in Table II. It is worth noting that, in the case of $k_c = 0.55$, the HCT-ROV performs slightly better (≈ 0.1 m) when controlled using thrusters only. This is due to the fact that the usage of the cables, which generate larger forces but are less precise, is always prioritized. However, for higher values of k_c the HCT-ROV actuated in an hybrid fashion outperforms the HCT-ROV actuated by thrusters only.

Another aspect considered during the tests is the quality of the estimation of the position of the ROV when using the CDPR forward kinematics presented in Section II-A. In particular, the depth z_i and the attitude $\{\phi, \theta, \psi\}$ are assumed to be known (estimated from sensors in the underwater vehicle) while the positions x_i and y_i are estimated thanks to the CDPR forward kinematics. Fig. 7 shows the error between the real position and the estimated one during the heavy lifting operation with $m_l = 2000$ kg. Since the errors are always smaller than 0.1 m, with RMS values equal to $rms_x = 0.0506$ m and $rms_y = 0.0499$ m, the position estimation is considered acceptable and thus useful.

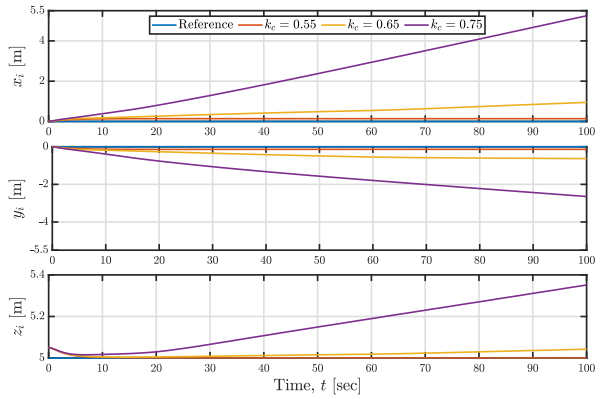

Fig. 5: Time evolution of the underwater vehicle position during hovering when it is actuated only by thrusters.

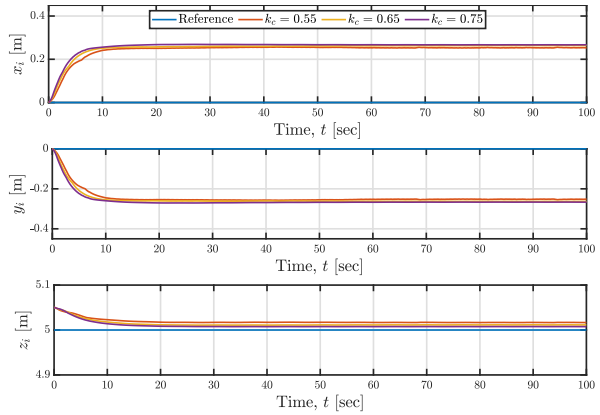

Fig. 6: Time evolution of the underwater vehicle position during hovering when it is actuated by thrusters and cables.

TABLE II: Hovering operation steady state position errors for the HCT-ROV controlled by both thrusters and cables.

k_c [m/s]	sse_x [m]	sse_y [m]	sse_z [m]
0.55	0.253	−0.252	0.016
0.65	0.26	−0.26	0.011
0.75	0.267	−0.266	0.007

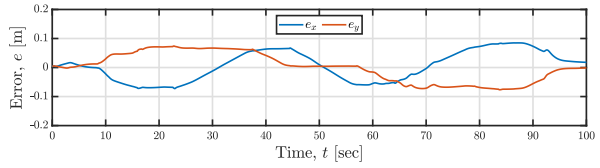

Fig. 7: Position estimation error using the forward kinematics presented in Section II-A.

VI. CONCLUSION AND FUTURE WORK

In this work, the control architecture of a HCT-ROV and a control allocation algorithm were presented. A full HCT-ROV model was implemented in a multibody real-time simulation software in order to analyze the performances of the system in two different real world scenarios, as well as to analyze the quality of the underwater vehicle position estimation provided by the forward kinematics of the cable robot. In future works, the case in which the floating platform is not fixed but is affected by oscillatory motion generated by waves will be considered. Moreover, analyses of the performances of HCT-ROV with smaller underwater vehicles will be carried out. Finally, the development of a more sophisticated controller and the realization of a physical prototype in order to perform real world experiments are also envisaged.

REFERENCES

[1] R. Bogue, "Underwater robots: a review of technologies and applications," *Industrial Robot: An International Journal*, 2015.

[2] G. Antonelli, *Underwater robots*. Springer, 2014, vol. 3.

[3] G. El-Ghazaly, M. Gouttefarde, and V. Creuze, "Hybrid cable-thruster actuated underwater vehicle-manipulator systems: A study on force capabilities," in *2015 IEEE/RSJ International Conference on Intelligent Robots and Systems (IROS)*. IEEE, 2015, pp. 1672–1678.

[4] C. Gosselin, "Cable-driven parallel mechanisms: state of the art and perspectives," *Mechanical Engineering Reviews*, vol. 1, no. 1, p. DSM0004, 2014.

[5] J.-B. Izard, A. Dubor, P.-E. Hervé, E. Cabay, D. Culla, M. Rodriguez, and M. Barrado, "Large-scale 3d printing with cable-driven parallel robots," *Construction Robotics*, vol. 1, no. 1, pp. 69–76, 2017.

[6] D. Q. Nguyen, M. Gouttefarde, O. Company, and F. Pierrot, "On the analysis of large-dimension reconfigurable suspended cable-driven parallel robots," in *2014 IEEE international conference on robotics and automation (ICRA)*. IEEE, 2014, pp. 5728–5735.

[7] J.-P. Merlet, "On the real-time calculation of the forward kinematics of suspended cable-driven parallel robots," in *14th IFToMM World Congress on the Theory of Machines and Mechanisms*, 2015.

[8] V. L. Nguyen and R. J. Caverly, "Cable-driven parallel robot pose estimation using extended kalman filtering with inertial payload measurements," *IEEE Robotics and Automation Letters*, vol. 6, no. 2, pp. 3615–3622, 2021.

[9] M. B. Larsen, "Synthetic long baseline navigation of underwater vehicles," in *OCEANS 2000 MTS/IEEE Conference and Exhibition. Conference Proceedings (Cat. No. 00CH37158)*, vol. 3. IEEE, 2000, pp. 2043–2050.

[10] T. Fossen, *Marine Control Systems: Guidance, Navigation and Control of Ships, Rigs and Underwater Vehicles*. Marine Cybernetics, 2002.

[11] V. Schmidt and A. Pott, "Implementing extended kinematics of a cable-driven parallel robot in real-time," in *Cable-driven parallel robots*. Springer, 2013, pp. 287–298.

[12] M. I. Lourakis *et al.*, "A brief description of the levenberg-marquardt algorithm implemented by levmar," *Foundation of Research and Technology*, vol. 4, no. 1, pp. 1–6, 2005.

[13] T. I. Fossen, "How to incorporate wind, waves and ocean currents in the marine craft equations of motion," *IFAC Proceedings Volumes*, vol. 45, no. 27, pp. 126–131, 2012, 9th IFAC Conference on Manoeuvring and Control of Marine Craft.

[14] CM Labs Simulations, "Vortex studio's multibody dynamics engine."

[15] K. M. Lynch and F. C. Park, *Modern robotics*. Cambridge University Press, 2017.

[16] M. Bodson, "Evaluation of optimization methods for control allocation," *Journal of Guidance, Control, and Dynamics*, vol. 25, no. 4, pp. 703–711, 2002.

[17] M. W. Oppenheimer, D. B. Doman, and M. A. Bolender, "Control allocation for over-actuated systems," in *2006 14th Mediterranean Conference on Control and Automation*. IEEE, 2006, pp. 1–6.

[18] T. A. Johansen and T. I. Fossen, "Control allocation—a survey," *Automatica*, vol. 49, no. 5, pp. 1087–1103, 2013.

[19] J. Virnig and D. Bodden, "Multivariable control allocation and control law conditioning when control effectors limit," in *Guidance, navigation, and control conference*, 1994, p. 3609.

[20] J. Nocedal and S. J. Wright, "Quadratic programming," *Numerical optimization*, pp. 448–492, 2006.

[21] J. A. Petersen and M. Bodson, "Constrained quadratic programming techniques for control allocation," *IEEE Transactions on Control Systems Technology*, vol. 14, no. 1, pp. 91–98, 2005.

[22] O. Härkegård, "Dynamic control allocation using constrained quadratic programming," *Journal of Guidance, Control, and Dynamics*, vol. 27, no. 6, pp. 1028–1034, 2004.

[23] S. Bochkanov, "Alglib (www.alglib.net)."